P1.5 A VALIDATION TECHNIQUE FOR CERES MONTHLY MEAN EARTH RADIATION SCANNER DATA USING ERBS NONSCANNER MEASUREMENTS

Stéphanie A. Weckmann*, G. Louis Smith, and Martial P. Haeffelin
Virginia Polytechnic Institute and State University, Blacksburg, Virginia
David F. Young, Bruce A. Wielicki, Richard N. Green, and Takmeng Wong
NASA /Langley Research Center, Hampton, Virginia

1. INTRODUCTION

The first Clouds and Earth's Radiant Energy System (CERES) (Wielicki et al. 1996) instrument was launched on board the Tropical Rainfall Measuring Mission (TRMM) satellite on November 27, 1997. The Earth Radiation Budget Satellite (ERBS) was placed in orbit in October 1984 as part of the Earth Radiation Budget Experiment (ERBE) (Barkstrom 1984). Whereas the narrow field of view (NFOV) scanning radiometers on board ceased taking measurements in 1990, the wide field of view (WFOV) nonscanning radiometers continue to operate to this date (Bush et al. 1999). It provides both instantaneous and monthly fluxes of the emitted longwave (LW) and reflected shortwave (SW). The ERBS WFOV data is the best current data record available to validate the new CERES monthly mean data product. The WFOV has already been used to validate the instantaneous ERBE and CERES NFOV radiances (Rutan et al. 1999). Because of its unique 14-year data record of LW and SW radiation the WFOV data set is a perfect validation link between the ERBE and CERES NFOV measurements.

In this paper, the ERBS WFOV monthly mean flux estimates are used as a validation tool for CERES ERBE-like monthly mean data. Specifically, a validation technique is developed to compare the WFOV to the 59-month historical ERBS NFOV monthly mean products. This validation technique is then applied to both the current ERBS WFOV and CERES monthly means products and the consistency between the two data sets is examined.

2. DATA

Three sets of data are used to complete the analysis:

- ERBS 2.5-deg. NFOV monthly means from the S-4G data product (March 1985 to January 1990),
- CERES ERBE-like 2.5-deg. NFOV monthly means from the ES-4G data product (January and February 1998),
- ERBS 10-deg. WFOV monthly mean shape factor data from the S-10N data product (March 1985 to January 1990, January and February 1998).

Due to a change in the spacecraft data format, only January and February 1998 WFOV data are used in our analysis. The months of April through August 1998 are not yet processed.

3. ANALYSIS

3.1 Background

The WFOV and NFOV radiometers both observe the same radiation field and should produce monthly fluxes that are very similar. One way to effectively compare these two data sets is to determine a scatter plot. A slope is obtained by performing a linear regression on it. A slope of 1 is an indication of good consistency between the two data sets. The further the slope is from 1 the less consistent the two data sets.

In our attempt to validate CERES monthly means, we first looked at the LW and SW slopes obtained from the scatter plots of the 59 months of ERBS 5-deg. numerical filter WFOV fluxes versus ERBS NFOV fluxes. Figure 1 shows the time series of the SW slope between the latitudes 40 N and 40 S. This time series reveals a semi-annual cycle, which also exists for the LW (not shown). The slope is maximum at the winter and summer solstice and minimum at the Autumnal and Vernal Equinox.

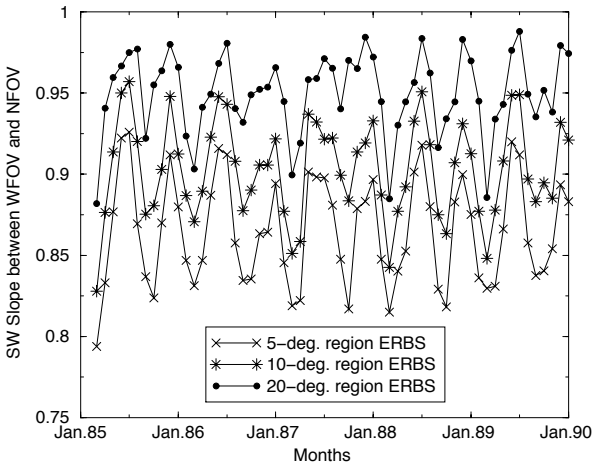

Figure 1. Time series of the shortwave slopes obtained from ERBS WFOV/NFOV scatter plots between 40 N and 40 S latitudes.

* Corresponding author address: Stéphanie Weckmann, NASA/Langley Research Center, Mail Stop 420, Hampton, VA 23681-2199
E-mail: s.a.weckmann@larc.nasa.gov

After investigating various parameters such as temporal sampling, the WFOV spatial resolution is believed to be responsible for this seasonal cycle. The WFOV radiometer observes the full Earth disc at once, whereas the NFOV has a spatial resolution of about 40 km at nadir. In a first attempt to remove the effect of the different spatial resolutions between the two instruments, we averaged the NFOV 2.5-deg. fluxes over 10-deg. and 20-deg. regions successively. In this manner, by averaging the NFOV data over a larger area, the two data sets become more spatially consistent. Figure 1 shows that even though the mean slope gets closer to 1 the semi-annual cycle is still showing after reducing the resolution to areas as large as 20 degrees.

3.2 Formulation of Weighted-Mean Flux

The results of Figure 1 demonstrate that simple averages of NFOV 2.5-deg. monthly means over larger regions do not match well the WFOV 10-deg. monthly means. We have developed a formulation to correct this domain difference by a weighted-mean of the NFOV fluxes over the larger domain associated with the WFOV flux. At a point defined by latitude Θ and longitude Φ we can define a weighted-mean flux by

$$\overline{F}(\Theta,\Phi) = \frac{\sum_{i,j} w_{i,j} F_{i,j}}{\sum_{i,j} w_{i,j}} \qquad (1)$$

where $w_{i,j}$ are the weights, $F_{i,j}$ are the NFOV fluxes, and i,j correspond to all 2.5-deg. regions within the domain of the WFOV measurement.

An examination of the data showed that the WFOV measurements were uniformly distributed over a 10-deg. region in the course of a month. Therefore, we want to define a uniform set of NFOV fluxes over the same 10-deg. region and average them. This was done by dividing the 10-deg. region into 100 1-deg. regions and computing the NFOV weighted-mean flux by (1) for each 1-deg. region. And finally, we area averaged the 100 fluxes to get a pseudo-WFOV flux based on NFOV fluxes.

We can derive the weights from the WFOV measurement equation given by (Green 1983)

$$m(\Theta_k,\Phi_k) = \pi^{-1} \int_{FOV} F(\Theta,\Phi)\, R(\Theta,\Phi,\theta) \cos\alpha \, d\Omega \qquad (2)$$

where α is the nadir angle in Figure 2, $\cos\alpha$ is the WFOV instrument response, R is the angular distribution model (ADM) for emitted radiance at viewing zenith θ, Ω is solid angle, and the integration is over the FOV or the domain of the WFOV. We can express (2) in terms of surface area S as

$$m(\Theta_k,\Phi_k) = \pi^{-1} \int_{S} F(\Theta,\Phi)\, R(\Theta,\Phi,\theta) \cos\alpha \frac{\cos\theta \, dS}{r^2} \qquad (3)$$

where r is the distance between the satellite and the TOA as shown in Figure 2. After discretization (3) becomes

$$m(\Theta_k,\Phi_k) = \sum_{i,j} w_{i,j} F_{i,j} \qquad (4)$$

where the weights are

$$w_{i,j} = \pi^{-1} R_{i,j} \cos\alpha_{i,j} \frac{\cos\theta_{i,j}}{r_{i,j}^{\,2}} \Delta S \cos\Theta_i \qquad (5)$$

and where ΔS is a constant such that $\Delta S \cos\Theta_i$ is the area of the ij[th] 2.5-deg. region. Thus, from (4) we see that the WFOV measurement weights TOA flux $F_{i,j}$ by $w_{i,j}$ and we will weight the NFOV fluxes the same by (1).

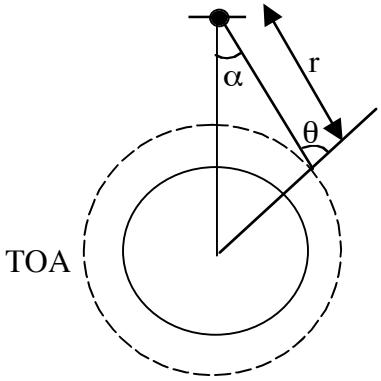

Figure 2. Geometry of the WFOV measurement

The weights in (5) have been derived for LW radiation and contain R, the LW ADM, which defines anisotropy such that the radiance I is given by $I = \pi^{-1} F R$. In general, R is a function of cloud amount. The R is incorporated in the computation of the instantaneous TOA fluxes from the radiance measurements. However, since we are applying the weights to monthly mean fluxes that are composed of various cloud amounts, it is not clear what value of R to use for the weights. For simplicity in this analysis we assume Lambertian radiation (R=1) and apply the weights to both SW and LW fluxes.

For our analysis with weighted fluxes we have used the 10-deg. region shape factor WFOV fluxes and not the 5.0-deg. region numerical filter fluxes. The shape factor fluxes allow us to interpret the flux from a single measurement (Green and Smith 1991). The numerical filter fluxes are derived from a more advanced method

that involves a set of measurements so that it is not appropriate for weighted fluxes.

4. RESULTS AND DISCUSSION

The formulation of the weights used to create a pseudo-WFOV flux is applied to the NFOV monthly fluxes for both ERBS and CERES and for both LW and SW monthly mean fluxes. The earlier ERBS analysis was between 40 N and 40 S latitudes. Because of CERES restricted latitudinal coverage, the weights can not be applied on the 10-deg. regions higher than 20 N and 20 S latitudes. In addition, the ERBS altitude dropped 20 km between 1990 and 1998. This drop was taken into account in the computation.

Figures 3a and 3b show the LW and SW slopes for the 59 months of ERBE before (bottom) and after (top) the weighting technique is applied.

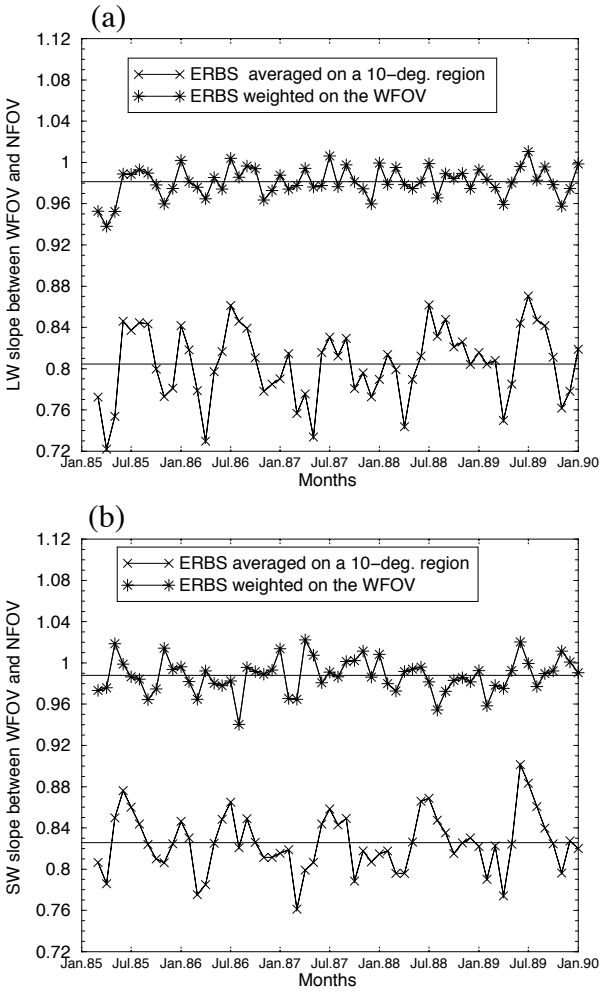

Figure 3. Effect of the weighting technique on the ERBE time series between March 1985 and January 1990 for (a) the longwave and (b) the shortwave flux slopes obtained from the WFOV/NFOV scatter plots between 20 N and 20 S latitudes.

A significant improvement in the mean slope is noticed after applying the weights. The mean slopes get closer to 1 thanks to this technique. Specifically, the LW slope is 0.98 and the SW slope is 0.99. The ADM variation is much larger for SW than for LW, so that it is probably fortuitous that the SW slope is closer to 1 than the LW slope. In addition, the semi-annual seasonal cycle is significantly attenuated. Standard deviations of 0.014 and 0.016 are found for the LW and SW, respectively. Note that the weighted-mean technique gives better results with LW than for the SW as far as the attenuation of the seasonal cycle. All these statistical results are gathered in Table 1. In view of these results, it is clear that the weighting technique removes most of the effects due to the spatial resolution differences between the WFOV and the NFOV.

TABLE 1. Slope statistical summary for ERBS for March 1985 to January 1990 for Figure 3.

20N-20S	Mean	Sigma	Range
SW original slope	0.83	0.028	0.140
SW weighted slope	0.99	0.016	0.083
LW original slope	0.80	0.035	0.15
LW weighted slope	0.98	0.014	0.073

Now that we have reasonable agreement between ERBS WFOV and NFOV data, we will apply the technique to ERBS WFOV and CERES NFOV. In applying this technique to CERES ERBE-like monthly means, we computed a 4-year mean slope with the ERBE historical data (from March 1985 to February 1989) between 20 N and 20 S latitudes. Figures 4a and 4b show the 4-year mean slope for LW and SW fluxes, respectively, with the lines of maxima and minima slope. Also plotted are January and February 1998 CERES data before the weighting technique is applied (circle) and after (triangle).

It is clear from Figures 4a and 4b that the weighting technique tends to eliminate the semi-annual cycle. The two CERES months added on those figures are a little offset especially for the month of February for both the LW and SW. We obtained a slope of 0.94 and 1.01 for the SW January and February, respectively, and 1.01 and 0.95 for the LW January and February, respectively. This offset might be explained by CERES and ERBS different orbits involving a different temporal sampling in the monthly means. In addition, January and February 1998 are two months when the El Niño index was extremely strong. So, we will have to wait for the rest of ERBS WFOV (April to August 1998) data to be processed in order to draw more conclusions. Nevertheless, those results are in good agreement with those presented by Rutan (1999) who found slopes of 0.98 and 1.11 for the LW and SW daytime for the combined 2 months.

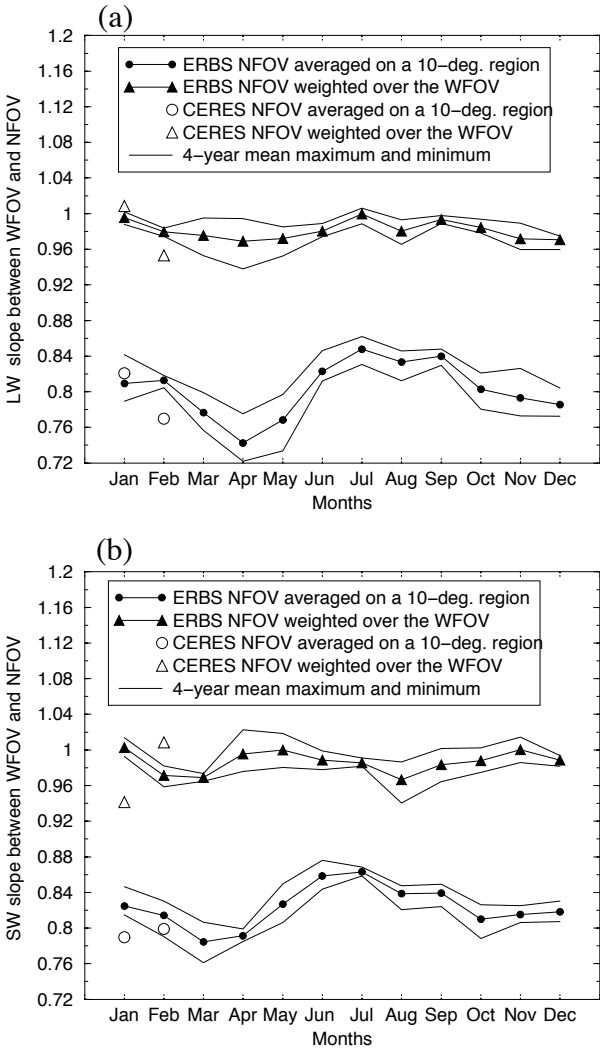

Figure 4. Effect of the weighting technique on (a) longwave and (b) shortwave WFOV/NFOV 4-year mean slope, as well as on CERES January and February 1998 slope between latitudes 20 N and 20 S.

5. CONCLUDING REMARKS

A validation technique is presented for comparing narrow field of view, scanner fluxes and wide field of view, nonscanner fluxes. The scanner fluxes are time averaged, monthly mean fluxes on a 2.5-deg. regional scale and the nonscanner fluxes are time averaged, monthly mean fluxes on a 10-deg. scale. Replacing the scanner flux with a weighted mean flux over the area observed by the nonscanner allows for direct comparison of the two data sets. The weights are derived from the nonscanner measurement equation so that the scanner and nonscanner both have the same weighting. Essentially, the scanner resolution is reduced to match the nonscanner resolution.

The technique was shown to work by applying it to ERBS nonscanner and scanner fluxes. The technique was then applied to ERBS nonscanner and CERES scanner fluxes. Only two months of ERBS fluxes were available for this analysis so that a full comparison between ERBS and CERES must wait until additional months are processed. However, the paper has shown that the 14-year ERBS nonscanner data set can be used to validate CERES data against the historical ERBS data of a decade earlier.

6. REFERENCES

Barkstrom B. R., 1984: The Earth Radiation budget Experiment (ERBE), Bull. Amer. Meteor. Soc., **65**, 1170-1185.

Bush, K. A., G. L., Smith, D. A. Rutan, B. R. Barkstrom, and D. Young, 1999: The ERBS 13-year Data Record, Proc. 3-rd Symp. Integrated Observing Systems, Amer. Met. Soc., January.

Green, R. N., 1983: Accuracy and Resolution of Earth Radiation Budget Estimates. J. Atmos. Sciences, **40**, 977-985.

_____, R. N., G. L. Smith, 1991: Shortwave Shape Factor Inversion of Earth Radiation Budget Observations. J. Atmos. Sciences, **48**, 390-402.

Rutan, D. A., G. L. Smith, T. P. Charlock, and R. N. Green, 1999: Early Intercomparison of CERES and ERBE Results, Proc. 3-rd Symp. Integrated Observing Systems, Amer. Met. Soc., January.

Wielicki, B. A., B. R. Barkstrom, E. F Harrison, R. B. Lee III, G. L. Smith, and J. E. Cooper, 1996: Clouds and the Earth's Radiant Energy System (CERES): an Earth Observation System Experiment, Bull. Amer. Met. Soc., **77**, 853-868.